

OPTIMIZATION OF WELD BEADS FORMED WITH AND WITHOUT USING FLUX OF ALUMINIUM ALLOY AA6082 USING ANOVA TECHNIQUES

Harish Chandra Dhaker¹, Suryabhan Kumar², Kumarpal Singh³, Pankaj Jain⁴

¹Research Scholar, Department of Mechanical Engineering, Aryabhata College of Engineering and Research Center, Ajmer Rajasthan India.

^{2,3,4}Asst. Professor, Department of Mechanical Engineering, Aryabhata College of Engineering and Research Center, Ajmer Rajasthan India.

ABSTRACT

This study investigates the effect of activated flux on the microstructure and weld bead geometry of Al-Mg-Si alloy AA6082 welded using the CMT process. ER4043 filler wire was used to create welds on 3 mm thick AA6082 plates. Various process parameters, including current (80, 100, and 110 A) and welding speed (30, 40, and 50 cm/min), were tested, while the nozzle tip distance and shielding gas flow rate were kept constant at 10 mm and 15 l/min, respectively. Optical microscopy was employed to examine the microstructural features of the welds. The results showed that welds made with activated flux exhibited increased penetration and dilution, along with higher micro-hardness compared to those made without activated flux.

Keywords: CMT, AA6082, ER4043, Weld bead geometry, Activated flux.

1. INTRODUCTION

Fusion welding is widely recognized as a key technique for enhancing innovative and sustainable production across various manufacturing sectors. Aluminium alloys, in particular, have garnered significant attention for their potential to create cost-effective, lightweight structures that offer excellent strength and stiffness. These properties make them ideal for modern industrial applications such as automotive manufacturing, aerospace, and shipbuilding. While pure aluminium is a versatile material, its inherent strength may not be sufficient for applications requiring high durability. To address this, aluminium is often alloyed with other elements to produce materials that are considerably stronger and more suitable for demanding industrial uses [1]. An "alloy" is a blend of different metallic elements designed to enhance the material's strength and durability. Depending on the intended application, pure aluminium is commonly alloyed with elements like silicon, manganese, tin, copper, and magnesium. With the right combination of alloying elements, aluminium can become significantly stronger, and in some cases, even outperform steel. Additionally, alloys provide a more cost-effective solution while offering many of the benefits of pure aluminium.

Aluminium alloys, particularly those in the 6000 series like AA6082, are widely used in industries such as aerospace, automotive, and construction due to their excellent combination of strength, corrosion resistance, and lightweight properties. These alloys are often welded in manufacturing processes that demand precision and high-quality joints. Among various welding techniques, Cold Metal Transfer (CMT) has gained significant attention in recent years for its ability to achieve low heat input, minimal distortion, and superior control over the welding process, making it particularly suitable for welding thin sections of high-performance aluminium alloys [2]. The CMT process is a modified version of traditional Gas Metal Arc Welding (GMAW), where the filler wire is intermittently fed into the weld pool with controlled retracting and advancing movements. This precise control of wire feed helps in reducing heat input, preventing excessive melting, and minimizing spatter. The process is well-suited for welding materials like AA6082, which are sensitive to heat-related defects like porosity and excessive grain growth [3].

Despite its advantages, the quality of welds produced by CMT is highly dependent on several process parameters, including welding current, travel speed, and arc length. In order to achieve optimal weld bead geometry, minimize defects, and enhance mechanical properties, it is essential to optimize these parameters. Previous research has indicated that the variation of welding parameters can significantly affect the weld's microstructure, hardness, penetration, and dilution. This study focuses on the optimization of welding parameters to investigate their effect on the weld bead characteristics of AA6082 aluminium alloy using the CMT process. Specifically, it aims to analyze the impact of welding current and welding speed on the quality of the welds, including the microstructural features and mechanical properties.

By understanding the influence of these parameters, this research seeks to contribute to the optimization of the CMT process for high-quality welds, with potential applications in industries where performance, reliability, and structural integrity are critical [4, 5].

2. MATERIALS AND EXPERIMENTAL WORK

2.1 Materials

AA6082 is a highly regarded structural alloy and is the strongest of the 6000 series aluminium alloys. Its composition mainly includes silicon and manganese. Known for its excellent machinability, it also offers outstanding properties like weldability, cold machinability, and corrosion resistance. ER4043 is a popular aluminium welding wire used in both Gas Tungsten Arc Welding (GTAW) and Gas Metal Arc Welding (GMAW) processes. It is a silicon-based wire primarily designed for welding aluminium alloys that contain silicon, such as those in the 6XXX series. Known for its excellent welding properties, ER4043 offers ease of use, minimal spatter, and good fluidity. It is particularly effective for welding thin materials and provides a good colour match with the base alloy. Additionally, ER4043 is a versatile wire suitable for both welding and brazing applications.

2.2 Experimental Work

In this study, a 3 mm thick AA6082 plate was used as the substrate material, and ER4043 filler wire (1.2 mm) was employed for welding on a CMT machine, as shown in Figure 1. Various test runs were conducted using different combinations of process parameters, with each experiment altering one parameter while keeping the others constant. The operating ranges of the process parameters used in this study are listed in Table 1. A Taguchi L9 orthogonal array was chosen for the design matrix, with tests conducted both with and without flux. This resulted in a total of 18 samples (9 samples without flux and 9 samples with flux), all produced using the CMT welding process.

Table 1: CMT PROCESS VARIABLES AND THEIR LEVELS

Welding Parameters	Units	Symbol	Levels		
			-1	0	1
Current	A	I	90	100	110
Welding speed	cm/min	S	30	40	50

The CMT machine is an advanced version of the GMAW machine, offering enhanced capabilities for more efficient welding. In this research, the TPS400i CMT machine (Figure 1) is used, with its detailed technical specifications provided in Table 3.5. One of the key advantages of CMT welding is the significant reduction in total welding time compared to traditional methods. A notable feature of this process is the short-circuit phase, which accounts for about one-fourth of the total welding time. During this phase, the welding current peaks before rapidly decreasing to nearly zero, a unique characteristic that distinguishes CMT welding from other techniques and contributes to its efficiency.

The integration of advanced technologies, such as high-speed digital process control (DPC) and a wire buffer, further enhances the CMT process. These technologies enable substantial cost and energy savings, typically ranging from 30% to 40% [6]. The DPC system works in synergy with the power source, automatically instructing the wire buffer to retract the filler wire during the short-circuit phase. This adjustment reduces the thermal heat input (THI), resulting in multiple benefits including minimal spatter, reduced distortion, and low dilution. These factors collectively improve the cost-effectiveness and energy efficiency of the CMT welding process [7, 8]. In the TPS400i CMT machine, a direct current electrode positive (DCEP) configuration is used. In this setup, the welding torch, which holds the wire electrode, is connected to the positive terminal of the power source, while the base metal (BM) is connected to the negative terminal. This configuration is also referred to as direct current reverse polarity (DCRP).



Figure 1: Experimental setup of CMT machine

Figure 2 shows the schematic of a fixture used to secure the AA6082 plate during welding. Prior to welding, each plate is cleaned with acetone ((CH₃)₂CO) to remove contaminants. A steel wire brush is then used to eliminate surface films and other impurities from the metal surface. The welding process utilizes argon gas (99.99% pure) as the shielding gas, with a contact tip-to-work distance (CTWD) of 10 mm, a 5 mm stick-out, and a 90° torch angle. The conventional bead-on-plate technique is employed to apply weld beads onto the AA6082 plates using a 1.2 mm diameter ER4043 wire (AlSi5%).

TABLE 2: DESIGN MATRIX

Sample Number	I (A)	S (cm/min)
1	90	30
2	90	40
3	90	50
4	100	30
5	100	40
6	100	50
7	110	30
8	110	40
9	110	50

TABLE 3: SPECIFICATION OF CMT MACHINE

Specifications	Units	Range
Maximum / minimum welding current	A / A	400/3
Welding current / Duty cycle [10 min/40°C]	A / %	400/40
Welding current / Duty cycle [10 min/40°C]	A / %	360/60
Welding current / Duty cycle [10 min/40°C]	A / %	320/100
Operating voltage	V	14.2-34.0
Open circuit voltage (OCV)	V	73
Main's frequency	Hz	50-60
Main's voltage	V	3 x 400
Main's fuse	A	35
Dimension / b	mm	300
Dimension / l	mm	706
Weight	kg	36.45
Degree of protection	-	IP23

The trials were conducted based on the Design of Experiments (DOE) outlined in Table 2. The Taguchi L9 design matrix was employed to determine the optimal parameters, with the number of trials specified accordingly. The results of these experiments are presented in Table 3. This approach leads to high-quality weld bead outcomes, such as superior strength, optimal penetration, and a smooth, aesthetically pleasing appearance, while minimizing the heat-affected zone (HAZ) and preventing deformation of the substrate material, especially in thin sheets.

The key dependent parameters for CMT welding include current, voltage, and wire feed rate, where changes in one parameter can affect the others. Prior to welding, the AA6082 sheets were cleaned using sandpaper to remove the oxide layer. The sheets were then aligned on a steel backing bar and secured at the ends with clamps to maintain proper positioning and spacing. Welding was performed using argon as the shielding gas, following the experimental setup detailed in Table 3.

After the weld bead was formed, a sample was extracted using wire EDM. The sample was then etched with Keller's reagent after being polished dry with emery paper, starting with 320 grit and progressing through 400, 600, 800, 1000, 1200, 1500, 2000, and 2500 grit for a fine finish.

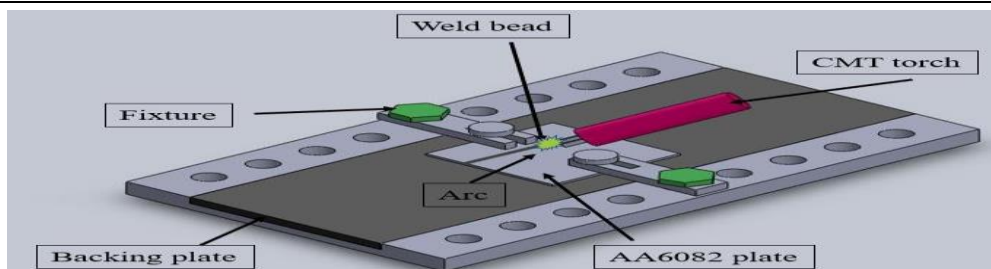


Figure 2: Schematic diagram of a fixture holding an AA6082 plate

3. EXPERIMENTAL RESULTS

In welding, optimizing process parameters like current and welding speed is essential to achieving the desired dilution ratio and weld quality [9]. The welding current, which represents the electrical energy flowing through the arc, influences both the temperature and heat input of the weld. A higher current typically leads to increased heat input and faster welding speeds, but it may also raise the likelihood of defects such as porosity and cracking.

3.1 Analysis of Variance (ANOVA)

ANOVA was applied to assess the influence of individual process parameters on the response variables—dilution percentage (%) and microhardness. Additionally, ANOVA helped identify the most statistically significant parameters affecting these outcomes. The ANOVA table provides a detailed analysis of the results for dilution and microhardness in the welded joints of AA6082 alloy, both with and without activated flux.

TABLE 4: L9 ORTHOGONAL ARRAY FOR THE SPECIMENS FORMED WITHOUT FLUX

S. No.	Current (A)	Welding speed (cm/min)	Dilution (%)	Penetration (mm)	Micro-hardness (HV)	Heat input (J/mm)
1	90	30	56.6	1.83	64.19	164.16
2	90	40	53.2	1.78	61.27	123.12
3	90	50	51.3	1.69	57.32	98.496
4	100	30	63.2	2.11	71.35	185.6
5	100	40	59.6	2.09	67.43	139.2
6	100	50	56.73	1.97	58.31	111.36
7	110	30	68.45	2.52	74.39	206.8
8	110	40	63.46	2.47	70.11	155.1
9	110	50	60.41	2.32	65.23	124.08

TABLE 5: L9 ORTHOGONAL ARRAY FOR THE SPECIMENS FORMED WITH FLUX

S. No.	Current (A)	Welding Speed (cm/min)	Dilution (%)	Penetration (mm)	Micro-Hardness (HV)	Heat Input (J/mm)
1	90	30	60.1	2.13	69.35	164.16
2	90	40	57.7	2.02	63.23	123.12
3	90	50	52.9	1.78	58.25	98.496
4	100	30	67.56	2.53	77.43	185.6
5	100	40	63.11	2.31	73.63	139.2
6	100	50	58.76	2.13	69.25	111.36
7	110	30	72.53	2.91	83.57	206.8
8	110	40	69.87	2.79	78.81	155.1
9	110	50	66.78	2.43	72.31	124.08

3.2 Optimization of Weld Beads Formed Without Using Flux

In the Taguchi optimization of weld bead samples produced without using active flux, the optimal process parameters with the highest S/N ratio were identified, indicating the maximum dilution and hardness [54]. Figures 3 and 4 display the S/N ratio curves for dilution and microhardness, respectively. The adequacy of the model was verified using the Analysis of Variance (ANOVA) technique. Table 6 shows that the maximum dilution occurs with a welding current at level 3 (110A) and a travel speed at level 1 (30 cm/min). Similarly, Table 9 indicates that the maximum hardness is achieved with a welding current at level 1 (90A) and a travel speed at level 3 (50 cm/min). The model's adequacy was further assessed using ANOVA. Tables 7 and 10 present the ANOVA results for dilution and microhardness of the weld beads formed without activated flux.

These tables provide key data such as sum of squares (SS), degrees of freedom (DF), mean square (MS)—which is the ratio of SS to DF—F-value, P-value, and percentage contribution. The F-value represents the ratio of variation between factors to the variation within factors, while the P-value indicates the probability that the observed effect is due to chance (with values below 0.05 considered statistically significant). The percentage contribution reflects the impact of each factor on the response variables. Adjusting the factor with the highest percentage contribution will have a significant influence on the output response, highlighting the sensitivity of that particular factor.

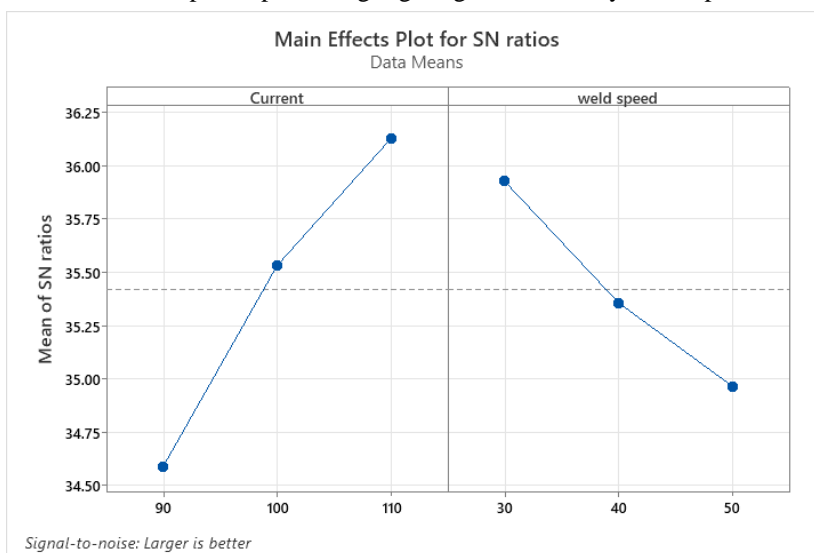


Figure 3: Plot between S/N ratio and current, weld speed of WFB for dilution

TABLE 6: RESPONSE TABLE OF S/N RATIO OF WFB FOR DILUTION

Level	Welding current	Travel speed
1	34.59	35.93
2	35.53	35.36
3	36.13	34.97
Delta	1.53	0.96
Rank	1	2

TABLE 7: ANOVA TABLE OF WFB FOR DILUTION

Source	DF	Contribution	Seq SS	Adj SS	Adj MS	F	P
Current	2	72.68%	0.000014	0.000014	0.000007	1819.82	0.000
Welding Speed	2	27.24%	0.000005	0.000005	0.000003	681.95	0.000
Error	4	0.08%	0.000000	0.000000	0.000000		
Total	8	100%	0.000019				

TABLE 8: MODEL SUMMARY OF WFB FOR TRANSFORMED RESPONSE

S	R-sq	R-sq (adj)	PRESS	R-sq (pred)	BIC
0.0000619	99.92%	99.84%	0.0000001	99.6%	-143.00

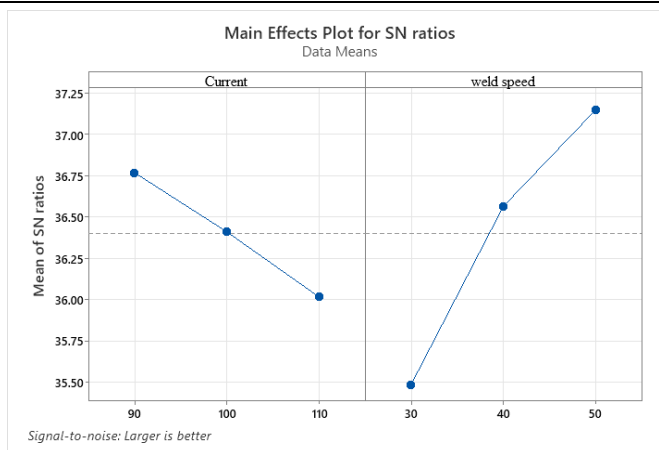


Figure 4: Plot between S/N ratio and current, weld speed of WFB for microhardness

TABLE 9: RESPONSE TABLE OF S/N RATIO OF WFB FOR MICROHARDNESS

Level	Current	Weld speed
1	36.77	35.49
2	36.41	36.56
3	36.02	37.15
Delta	0.75	1.66
Rank	2	1

TABLE 10: ANOVA TABLE OF WFB FOR MICRO-HARDNESS

Source	DF	Contribution	Seq SS	Adj SS	Adj MS	F	P
Current	2	15.99%	0.000003	0.000003	0.000001	24.34	0.006
Welding	2	82.69%	0.000013	0.000013	0.000007	125.84	0.001
Error	4	1.31%	0.000000	0.000000	0.000000		
Total	8	100%	0.000016				

TABLE 11: MODEL SUMMARY OF WFB FOR TRANSFORMED RESPONSE

S	R-sq	R-sq (adj)	PRESS	R sq (pred)	BIC
0.0002301	98.69%	97.37%	0.0000011	93.35%	-119.36

For dilution, welding current is the more dominant factor, contributing 72.68%, compared to welding speed, which contributes 27.24%. In contrast, for microhardness, welding speed is the more dominant factor, accounting for 82.69%, while welding current contributes just 15.99%. This is due to the lower P-values and higher F-values associated with welding speed.

The predicted R^2 values show good agreement with the adjusted R^2 values for all response parameters, with a difference of less than 0.2. This close match indicates that most data points are well-aligned with the regression model. The key distinction between adjusted R^2 and predicted R^2 lies in their interpretation. Adjusted R^2 identifies the independent variables that actually affect the dependent variable, while predicted R^2 assumes that the variation in the dependent variable is explained by each individual factor, giving an indication of the percentage of variation explained by the model.

Tables 8 and 11 present the model summary, showing that the R^2 values serve as a validation criterion. In this study, the model accounts for 99% of the variance in dilution and 93.5% of the variance in microhardness, indicating a high level of explanatory power for the predictor variables.

3.3 Optimization of weld Beads Formed Using Activated Flux

In the Taguchi optimization of weld bead samples produced using active flux, the optimal process parameters with the highest S/N ratio were identified, indicating the maximum dilution and hardness. Figures 5 and 6 display the S/N ratio curves for dilution and microhardness, respectively. The adequacy of the model was verified using the Analysis of Variance (ANOVA) technique. Table 12 shows that the maximum dilution occurs with a welding current at level 3

(110A) and a travel speed at level 1 (30 cm/min). Similarly, Table 15 indicates that the maximum hardness is achieved with a welding current at level 1 (90A) and a travel speed at level 3 (50 cm/min).

The model's adequacy was further assessed through ANOVA, and the results are presented in Tables 13 and 16 for dilution and microhardness of the weld beads formed using active flux. These tables provide key data such as the sum of squares (SS), degrees of freedom (DF), mean square (MS) - the ratio of SS to DF: F-value, P-value, and percentage contribution.

The F-value represents the ratio of variation between factors to the variation within factors, while the P-value indicates the probability of the observed effect being due to chance, with values below 0.05 considered statistically significant. The percentage contribution reflects the impact of each factor on the response variables. Adjusting the factor with the highest percentage contribution will significantly influence the output response, highlighting the sensitivity of that particular factor.

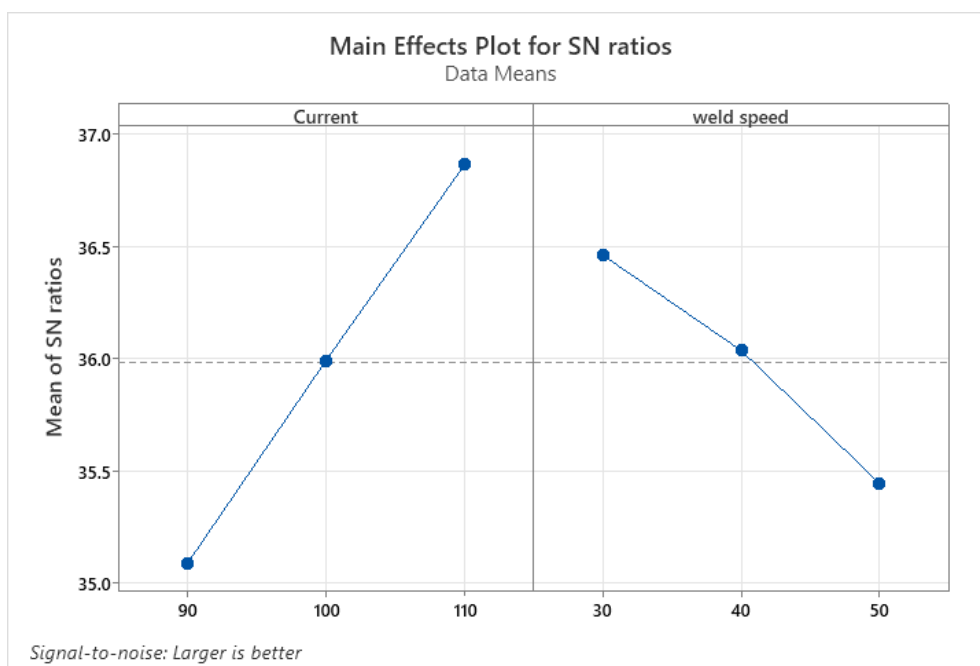


Figure 5: Plot between S/N ratio and current, weld speed of FB for dilution

TABLE 12: RESPONSE TABLE OF S/N RATIO OF FB FOR DILUTION

Level	Welding current	Travel speed
1	35.09	36.46
2	35.99	36.04
3	36.86	35.45
Delta	1.77	1.01
Rank	1	2

TABLE 13: ANOVA TABLE OF FB FOR DILUTION

Source	DF	Contribution	Seq SS	Adj SS	Adj MS	F-value	P-value
Current	2	75.50%	3946778	3946778	1973389	203.88	0.000
Welding Speed	2	23.76%	1241946	1241946	620973	64.16	0.001
Error	4	0.74%	38716	38716	9679		
Total	8	100%	5227440				

TABLE 14: MODEL SUMMARY OF FB FOR TRANSFORMED RESPONSE

S	R-sq	R-sq (adj)	PRESS	R sq (pred)	BIC
98.3824	99.26%	98.52%	196002	96.25%	114.03

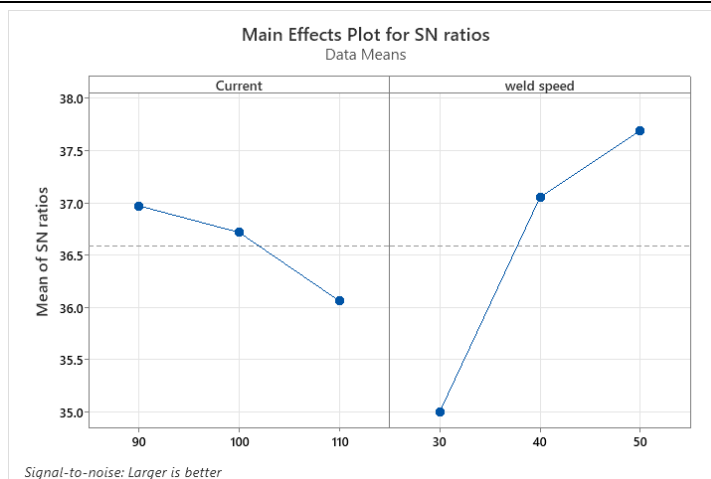


Figure 6: Plot between S/N ratio and current, weld speed of FB for microhardness

TABLE 15: RESPONSE TABLE OF S/N RATIO OF FB FOR MICROHARDNESS

Level	Current	Welding speed
1	36.97	35.01
2	36.72	37.05
3	36.06	37.69
Delta	0.91	2.68
Rank	2	1

TABLE 16: ANOVA TABLE OF FB FOR MICROHARDNESS

Source	DF	Contribution	Seq SS	Adj SS	Adj MS	F- value	P- value
Current	2	10.00%	0.017493	0.017493	0.008746	20.15	0.008
Welding speed	2	89.01%	0.155738	0.155738	0.077869	179.35	0.001
Error	4	0.99%	0.001737	0.001737	0.000434		
Total	8	100.00%	0.174968				

TABLE 17: MODEL SUMMARY OF FB FOR TRANSFORMED RESPONSE

S	R ²	R ² (adj)	PRESS	R ² (pred)	BIC
0.0208368	99.01%	98.01%	0.0087920	94.98%	-38.25

For dilution, welding current is the more dominant factor, contributing 75.50%, compared to welding speed, which contributes 23.76%. However, for microhardness, welding speed is the more dominant factor, accounting for 89.01%, while welding current contributes just 10.00%. This difference is attributed to lower P-values and higher F-values associated with welding speed. The predicted R² values show good agreement with the adjusted R² values for all response parameters, with a difference of less than 0.2. This close alignment suggests that most data points fall within the regression line. The key distinction between adjusted R² and predicted R² lies in their interpretation. Adjusted R² identifies the independent variables that truly affect the dependent variable, while predicted R² assumes that the variation in the dependent variable is explained by each individual factor, providing an estimate of the percentage of variation explained by the model. Tables 14 and 17 present the model summary, indicating that R² serves as a validation criterion. In this case, the model accounts for 96.25% of the variance in dilution and 94.98% of the variance in microhardness, demonstrating a high level of explanatory power for the predictor variables.

4. CONCLUSIONS

In this study, metal matrix composite samples were produced using an active flux and the Cold Metal Transfer (CMT) process. The main objective was to investigate the influence of SiC particles on grain orientation, grain evolution, and the mechanical properties of the welds, and to compare the results with samples welded without flux. The following key findings were made: Penetration and Bead Width: Weld beads produced using activated flux exhibited higher penetration and reduced bead width compared to those made without flux, under the same welding current and speed. Achieving sufficient dilution and penetration while minimizing heat input is critical for enhancing joint efficiency.

ACKNOWLEDGEMENT

The First author wish to express his thanks to the Principal, Aryabhata College of Engineering and Research Center, Ajmer, Rajasthan, India, to carry out the above work in Department of Mechanical Engineering and wish to express his sincere thanks to the Former Chairman Prof. Amit Shastri for their encouragement and support to undertake the present work and providing the facilities in Department of Mechanical Engineering. He also expresses his thanks to his colleagues in Department of Mechanical Engineering for their support.

5. REFERENCES

- [1] Elrefaey A, and Ross NG, "Microstructure and mechanical properties of cold metal transfer welding similar and dissimilar aluminium alloys", *Acta Metall. Sin- Engl.* 28 715-724, 2015.
- [2] Mcauley JW, "Global sustainability and key needs in future automotive design", *Environ. Sci. Technol.*, 37 5414- 5416, 2003.
- [3] Selvamani ST, Govindarajan P, Ajaymohan M, Hariharan SJ, and Vigneshwar M, "Correlation between Micro hardness and Microstructure of CMT Welded AA 7075 Al Alloy", In *IOP Conference Series: Materials Science and Engineering* 390 012058, 2018.
- [4] Totten GE, and MacKenzie DS, "Handbook of aluminium: vol. 1", *Physical metallurgy and processes*; CRC press, New York, 2003.
- [5] Kaufman JG, "Introduction to aluminium alloys and tempers", ASM international USA, 2000.
- [6] Mathers G, "The welding of aluminium and its alloys", Woodhead publishing England, 2002.
- [7] Summers, P.T., Chen, Y., and Rippe, C.M., "Overview of aluminum alloy mechanical properties during and after fires", *Fire Sci. Rev*, Vol. 4, No. 3, 2015
- [8] Connor LP, "Welding Handbook: Vol. 1: Welding Technology", *Welding Science and Technology*, 9th edition American Welding Society.
- [9] Taheri H, Kilpatrick M, Norvalls M, Harper WJ, Koester LW, Bigelow T, Bond LJ, "Investigation of Nondestructive Testing Methods for Friction Stir Welding. *Metals*", 9(6):624, 2019.
- [10] Liu, K., Jiang, X., Chen, S., "Effect of SiC addition on microstructure and properties of Al-Mg alloy fabricated by powder and wire cold metal transfer process", *Journal of Materials research & Technology*, 17:310-319, 2022.